1.57 MW peak power pulses generated by a diode-pumped Q-switched Nd:LuAG ceramic laser

Jian Ma (马 剑)[1,2], Tingting Lu (陆婷婷)[1], Xiaolei Zhu (朱小磊)[1,*], Benxue Jiang (姜本学)[3], Pande Zhang (张攀德)[2,3], and Weibiao Chen (陈卫标)[1]

[1]*Key Laboratory of Space Laser Communication and Detection Technology, Shanghai Institute of Optics and Fine Mechanics, Chinese Academy of Sciences, Shanghai 201800, China*
[2]*University of Chinese Academy of Sciences, Beijing 100049, China*
[3]*Key Laboratory of Materials for High Power Laser, Shanghai Institute of Optics and Fine Mechanics, Chinese Academy of Sciences, Shanghai 201800, China*
*Corresponding author: xlzhu@siom.ac.cn

Received October 16, 2017; accepted October 20, 2017; posted online November 9, 2017

The pulse characteristics of a laser diode dual-end-pumped electro-optic Q-switched Nd:LuAG ceramic laser at various repetition rates are presented. The largest output pulse energy of 11 mJ is realized at the repetition rate of 100 Hz with pump energy of 84.3 mJ, and the slope efficiency in respect to pump pulse energy is 18.6%. The single pulse peak power reaches up to 1.57 MW. Using Nd:LuAG ceramic as the amplification medium seeded by an Nd:YAG laser of 5.2 mJ, a 10.3 mJ amplified pulse is obtained with pump pulse energy of 42.8 mJ, corresponding to an extraction efficiency of 11.9%.

OCIS codes: 140.0140, 140.3380, 140.3480, 140.3540.
doi: 10.3788/COL201715.121402.

Transparent laser ceramics have attracted much interest for large volumes and short production periods with the possibility for complicated composite structure[1]. In recent years, Nd:LuAG ceramics have been fabricated[2–6], and the laser performances have been demonstrated[7–13]. In Ref. [14], Kuwano *et al.* demonstrated that LuAG had comparable mechanical and optical properties with YAG. Compared with Nd:YAG, Nd:LuAG is a promising gain medium for solid-state lasers due to the following advantages. First, Nd:LuAG owns longer fluorescence lifetime than that of Nd:YAG[15], which suggests that Nd:LuAG processes better energy storage capacity in high power scaling lasers[16]. Secondly, Nd:LuAG shows better thermo-optic performance because the atomic mass of Lu^{3+} ions is closer to the doping ions Nd^{3+} than Y^{3+} ions[10,17]. In 2015, Ye *et al.* reported diode-end-pumped continuous-wave (CW) Nd:LuAG ceramic lasers at 1064 and 1123 nm with $^4F_{3/2} \rightarrow {}^4I_{11/2}$ transition[7]. The optical properties and CW laser performance of 0.8 at.% Nd:LuAG transparent ceramic were investigated by Fu *et al.* in 2016[8]. In the same year, Ma *et al.* fabricated Nd:LuAG transparent ceramic composited with YAG and obtained CW laser output at 1064 nm[9]. Then, in 2017, they reported the fabrication of 2 at.% Nd:LuAG transparent ceramic and the CW laser performances[10]. In the same year, Yan *et al.* reported diode-pumped CW 1.4 μm eye-safe Nd:LuAG ceramic lasers[11], and Zhou *et al.* reported a diode-pumped Nd:LuAG ceramic laser operated at 1.83 μm[12]. All of the Nd:LuAG ceramic lasers introduced above were operated in the CW mode. Only, in 2015, Qiao *et al.* presented the Nd:LuAG ceramic laser both in the CW mode and electro-optical (EO)

Q-switched mode. Working in the Q-switched mode, laser pulse energy of 1.96 mJ was obtained with a pulse width of 4.8 ns, and the peak power was 0.41 MW[13].

In this Letter, we present a laser diode (LD) dual-end-pumped Q-switched Nd:LuAG ceramic laser with the highest pulse peak power (>1.5 MW) output so far, to the best of our knowledge. The characteristics of Nd:LuAG ceramic laser operated both in the free-running mode and Q-switched mode were investigated. In addition, the pulse amplification properties of Nd:LuAG ceramic were investigated in a master oscillator power amplifier (MOPA). This is the first laser amplifier using Nd:LuAG ceramic as a gain medium. The experimental results show that Nd:LuAG ceramic has the potential to generate high peak power laser pulses in diode-pumped lasers.

The Nd:LuAG transparent ceramic samples used in the experiments were fabricated by the solid-state reactive sintering method with the Nd^{3+}-ion doping concentration of 0.8 at.%. The fluorescence emission spectrum of the Nd:LuAG ceramic is shown in Fig. 1[13]. The main emission bands are found to be located at 900–960, 1060–1130, and 1350–1450 nm, which belong to the transitions of $^4F_{3/2} \rightarrow {}^4I_{9/2}$, $^4F_{3/2} \rightarrow {}^4I_{11/2}$, and $^4F_{3/2} \rightarrow {}^4I_{13/2}$, respectively. The highest emission peak is centered at about 1064 nm, belonging to the Stark transition R2 → Y3. The transmission of the Nd:LuAG ceramic sample at 1 μm was also measured, and the scattering coefficient was calculated to be about 0.04 cm^{-1}.

Two 4 mm × 3.6 mm × 12 mm Nd:LuAG ceramic slabs were anti-reflection (AR) coated at both 1064 and

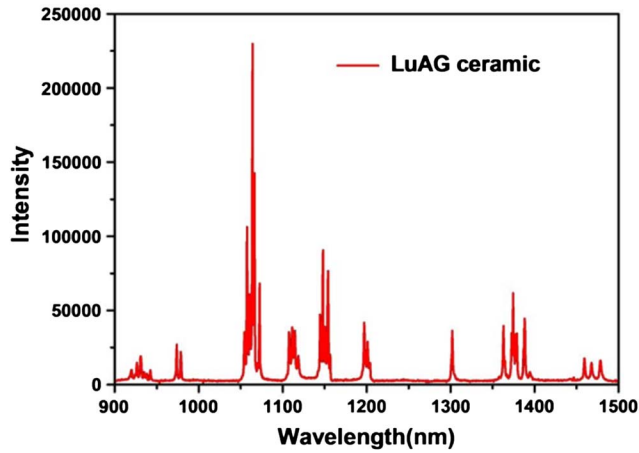Fig. 1. Fluorescence emission spectrum of the Nd:LuAG ceramic[13].

Fig. 3. (Color online) Output energy as a function of pump energy in the free-running mode and Q-switched mode.

808 nm on the 4 mm × 3.6 mm faces for dual-end-pumped operation. Nd:LuAG ceramic slabs were wrapped by indium foil and mounted on a water-cooled copper heat sink at 20℃. The pump source comprised two fiber-coupled 808 nm LDs with maximum 150 W peak power. The core diameter of the output fiber was 600 μm, and the numerical aperture (NA) was 0.17. The LDs were operated in the quasi-CW (QCW) mode with a pump pulse duration of 280 μs, determined by the fluorescence lifetime of Nd:LuAG ceramic. The schematic of the electro-optic Q-switched laser is shown in Fig. 2. The pump laser beam passed through 2:5 coupling lenses into the laser medium, with a pump beam waist of 1.5 mm in diameter. The laser was operated in a U-type folded cavity containing four mirrors. All of the cavity mirrors were plane–plane mirrors, and the coating parameters are shown in the note title of Fig. 2. The cavity length was 450 mm. A potassium dideuterium phosphate (KD*P) Pockels cell was used as the EO Q-switch with a polarizer and a quarter wave-plate. The laser properties at different repetition rates that varied from 100 to 500 Hz were investigated in detail with the same cavity parameters.

Figure 3 shows the output pulse energy at 1064 nm as a function of the pump pulse energy in the free-running and Q-switched modes at the repetition rate of 100 Hz. The slope efficiency was 35.5% in the free-running mode,
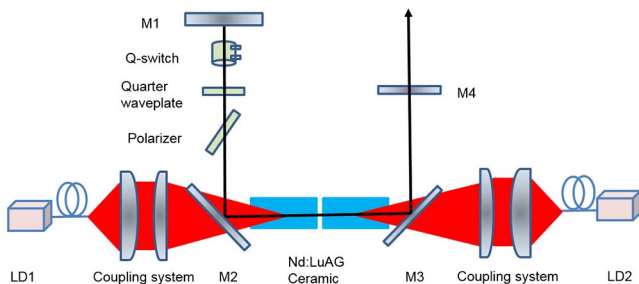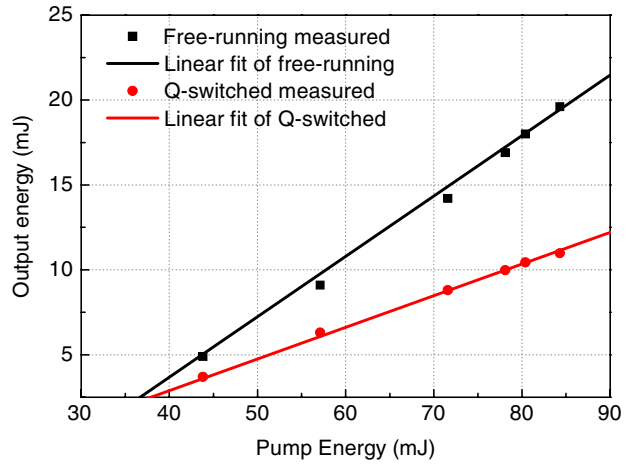
and the maximum output pulse energy of 19.6 mJ was obtained with 84.3 mJ incident pump energy, corresponding to optical-to-optical efficiency of 23.3%. The slope efficiency was 18.6% in the Q-switched mode, and the maximum output pulse energy of 11 mJ was obtained with optical-to-optical efficiency of 13%. The dynamic to static ratio was 56%. Similar EO Q-switched laser operation was carried out by our group using Nd:LuAG crystal as the laser medium in 2015[18]. The 13 mJ pulse energy at 1064 nm was obtained with a pulse width of 9 ns. By contrast, the Nd:LuAG ceramic approached comparable optical and laser performance to the Nd:LuAG crystal.

The output energy of the EO Q-switched Nd:LuAG ceramic laser that operated at a different repetition rate is shown in Fig. 4. The symbols show the experimental results, and the dotted lines are the fitting predictions. Both the pump energy threshold and the slope efficiency decreased with the increase of the repetition rate. The slope efficiency was 18.6% at 100 Hz, 17.5% at 150 Hz, 12.3% at 200 Hz, 10.9% at 250 Hz, and 10.7% at 500 Hz, respectively. The output laser pulse energy tends

Fig. 2. Schematic of the EO Q-switched Nd:LuAG ceramic laser: M1, high reflection (HR) at 1064 nm; M2 and M3, HR at 1064 nm and AR at 808 nm; M4, $T = 60\%$ at 1064 nm.
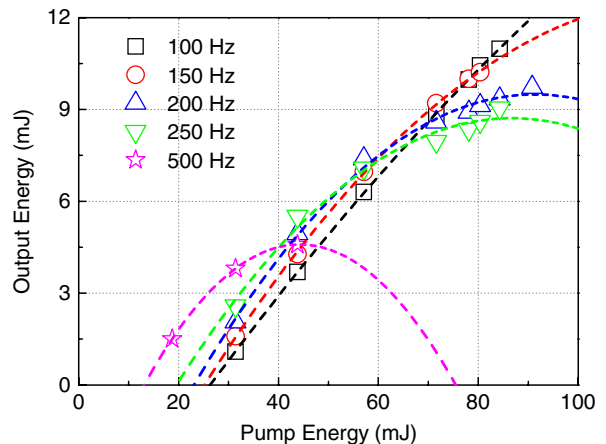

Fig. 4. (Color online) Output pulse energy as a function of pump energy.

to be saturated with a further increase of pump energy, and the saturation point occurs earlier at a high repetition rate. Such results are due to different thermal lens effects as well as thermal-induced birefringence and distortion.

The temperature distribution inside the laser medium has been studied by the finite-element method to determine the thermal lensing effect of Nd:LuAG ceramic. For a paraxial beam propagating in the z direction, the optical path difference (OPD) for one single trip due to a thermal-induced refractive index change is given by[19]

$$\mathrm{OPD}_T = \int_0^l \frac{\partial n}{\partial T} \Delta T(r)\, \mathrm{d}r. \quad (1)$$

The corresponding thermal focal length is

$$f_T^r = \frac{r^2}{2[\mathrm{OPD}(o) - \mathrm{OPD}(r)]c}, \quad (2)$$

where $\mathrm{OPD}(o)$ and $\mathrm{OPD}(r)$ represent the OPD of the slab center and edge, respectively. The horizontal (x direction) and vertical (y direction) thermal focal lengths are calculated and shown in Fig. 5. The thermal focal length is inversely proportional to the repetition rate with the same pump energy. The simulated result shows that the higher the repetition rate is, the smaller the thermal focal length is. At the repetition rate of 500 Hz, the thermal focal length is 0.5 and 0.6 m, respectively, in the x direction and y direction. Compared with a plano–plano cavity without any thermal lens, in which the laser mode matches well with the pump mode, the thermal lens effect of the laser medium makes the lasing mode smaller in size, resulting in a mismatch of the laser mode with the pump mode, which leads to lower slope efficiency.

The near-field beam profile at 100 Hz was detected to be near the Gaussian distribution with good uniformity and is shown in Fig. 6. However, the uniformity of the beam profile deteriorated when the repetition rate increased. The beam quality factor M^2 is measured at different repetition rates and is shown in Fig. 7. The beam quality
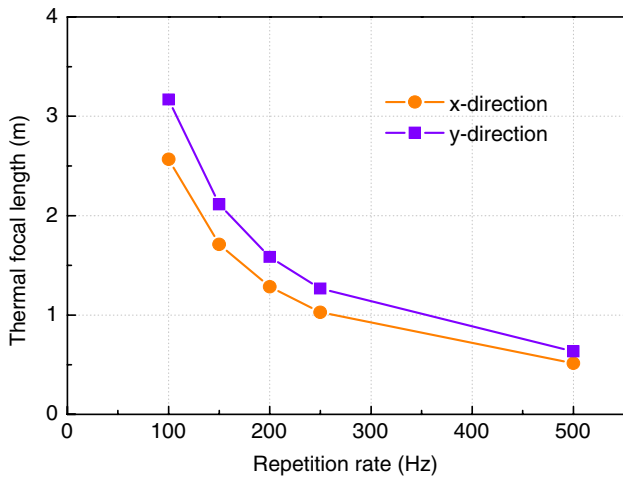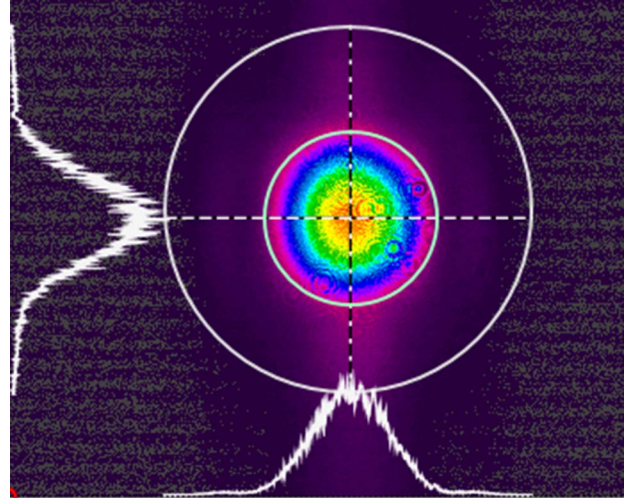

Fig. 6. Near-field beam profile with 11 mJ pulse energy at 100 Hz.
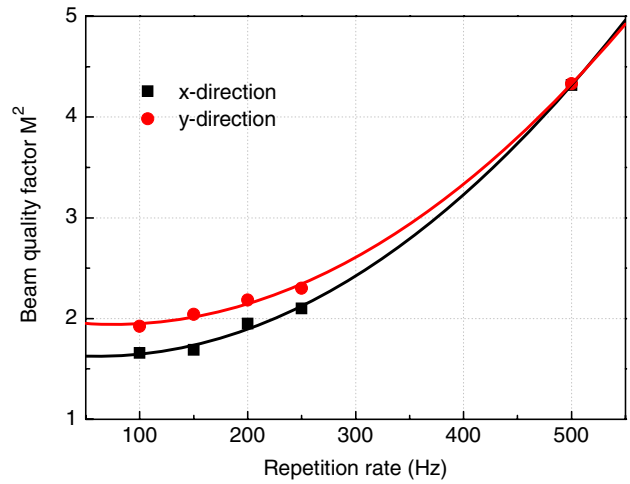

Fig. 7. (Color online) Beam quality factor M^2 versus repetition rate.

got worse with the increase of the repetition rate. At 100 Hz, the measured M_x^2 was 1.66, and M_y^2 was 1.92, while M_x^2 was 4.32, and M_y^2 was 4.33 at 500 Hz. The difference in the temperature distribution within the x plane and y plane inside the Nd:LuAG ceramic slabs might lead to the difference of the M^2 factor in two directions. At a high reflection rate, a more severe thermal dispersion and thermal-induced birefringence may result in the distortion of the laser beam and the degradation of the beam quality.

The typical temporal trace of EO Q-switched Nd:LuAG ceramic laser pulse is shown in Fig. 8. The pulse width was about 7 ns when the output pulse energy was 11 mJ at the repetition rate of 100 Hz, and the pulse peak power reached up to 1.57 MW. The center wavelength of laser pulses was 1064.48 nm.

Compared with the Nd:YAG medium, the fluorescence lifetime of Nd:LuAG is longer, and the emission cross section is also larger, indicating Nd:LuAG is a useful medium in high energy lasers. To investigate the power scaling

Fig. 5. (Color online) Simulated thermal focal length versus repetition rate.
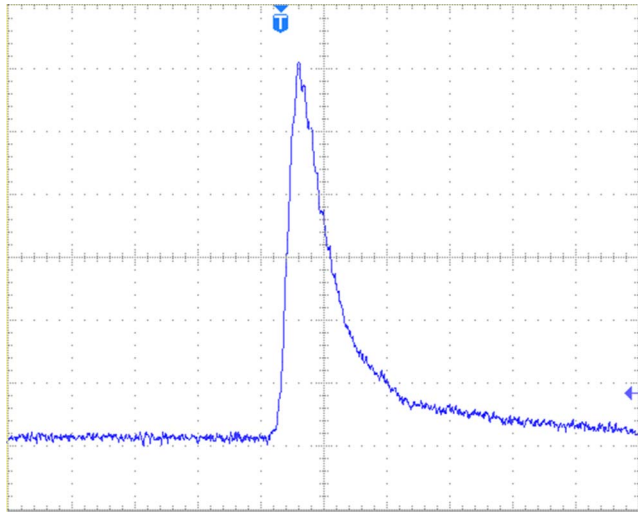
Fig. 8. Temporal trace of output laser pulse.

properties of Nd:LuAG ceramic, a MOPA experiment was carried out and seeded by a Q-switched Nd:YAG laser. In Fig. 9, LD1 for the Nd:YAG seed laser and LD2 for the Nd:LuAG ceramic amplifier were driven by the same power supply at 100 Hz with pump pulse duration of 280 μs. The pump beam waist of the amplifier stage was 1.5 mm in diameter, and the seed laser beam passed through the coupling lenses to obtain a 1.4 mm laser spot that matched the waist diameter of the pump beam. The same Nd:LuAG ceramic slabs used in the former EO Q-switched operation acted as a gain medium for the amplifier. The laser medium of the master oscillator is a $\Phi 4$ mm $\times$ 30 mm Nd:YAG crystal rod bonding with 5 mm un-doped YAG on each end to relieve the thermal effect, and the doping concentration of the 30-mm-long area is 0.3 at.%. The seed wavelength was 1064.38 nm, which is slightly different from that of the Nd:LuAG

ceramic oscillator, as we introduced previously to be 1064.48 nm.

The amplified pulse energy E_{output}, as a function of input seed pulse energy E_{seed}, and the stored energy E_{stored} in the gain medium can be simulated based on the Frantz–Nodvik formula[20]:

$$E_{\text{output}} = E_s A \left\{ 1 + \left[\exp\left(\frac{E_{\text{seed}}}{A E_s}\right) - 1 \right] \exp\left(\frac{E_{\text{stored}}}{A_P E_s}\right) \right\}, \tag{3}$$

where E_s is the saturation fluence determined by $E_s = h\upsilon/\sigma$. h refers to the Planck Constant, υ refers to laser frequency, and σ refers to the emission cross section of Nd:LuAG at 1064 nm. The emission cross section valued at 29×10^{-20} cm^2[10,21] is taken into calculation, resulting in $E_s = 0.64$ J/cm^2. A is the spot area of the seed laser, and A_p is the pump spot area.

The seed laser energy is shown in Fig. 10 and is denoted by the black squares. The red dots show the amplified results, and the solid line represents the theoretical calculated amplification results, which are in good agreement with the experimental results. With pump energy of 42.8 mJ and the seed energy of 5.2 mJ, the Nd:LuAG ceramic amplifier generated laser pulses of 10.3 mJ at 100 Hz, corresponding to extraction efficiency of 11.9%. The laser amplification results shows that Nd:LuAG ceramic is capable for power scaling, even when the emitting central wavelength of Nd:LuAG ceramic (1064.48 nm) is slightly different from that of the seed laser (1064.38 nm).

In conclusion, the Q-switched pulse characteristics and amplification performance of Nd:LuAG ceramic are demonstrated. The largest output pulse energy of 11 mJ is realized in the Q-switched laser, and the single pulse peak power reaches up to 1.57 MW. The Nd:LuAG ceramic amplifier generates 10.3 mJ laser pulses with the magnification of two times. The research results
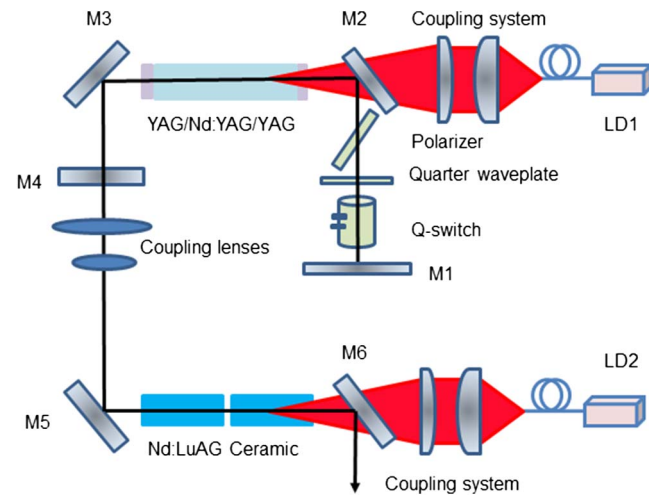

Fig. 9. Schematic of MOPA system: M1, HR at 1064 nm; M2, M3, M5, and M6, HR at 1064 nm and high transmission (HT) at 808 nm; M4, $T = 60\%$ at 1064 nm.
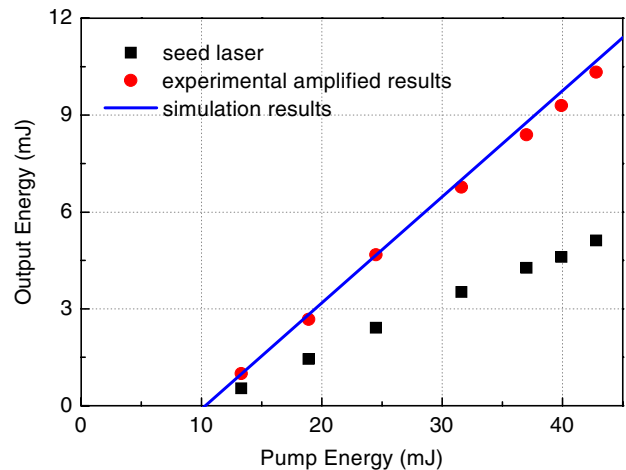

Fig. 10. Experimental and stimulated output energy of Nd:LuAG ceramic amplifier as a function of the pump energy.

proves that Nd:LuAG ceramic can be a potential medium in high energy and high peak power lasers.

References

1. A. Ikesue and Y. L. Aung, Nat Photon. **2**, 721 (2008).
2. N. Wagner, B. Herden, T. Dierkes, J. Plewa, and T. Justel, J. Eur. Ceram Soc. **32**, 3085 (2012).
3. Y. Zhang, M. Cai, B. X. Jiang, J. T. Fan, C. L. Zhou, X. J. Mao, and L. Zhang, Opt. Mater. Express **4**, 2182 (2014).
4. P. D. Zhang, B. X. Jiang, J. T. Fan, X. J. Mao, and L. Zhang, Opt. Mater. Express **5**, 2209 (2015).
5. P. D. Zhang, B. Y. Chai, B. X. Jiang, Y. G. Jiang, S. L. Chen, Q. J. Gan, J. T. Fan, X. J. Mao, and L. Zhang, J. Eur. Ceram Soc. **37**, 2459 (2017).
6. L. Bonnet, R. Boulesteix, A. Maitre, C. Salle, V. Couderc, and A. Brenier, Opt. Mater. **50**, 2 (2015).
7. Y. L. Ye, H. Y. Zhu, Y. M. Duan, Z. H. Shao, D. W. Luo, J. Zhang, D. Y. Tang, and A. A. Kaminskii, Opt. Mater. Express **5**, 611 (2015).
8. Y. L. Fu, J. Li, Y. Liu, L. Liu, T. X. Xu, H. H. Yu, H. Zhao, H. J. Zhang, and Y. B. Pan, J. Eur. Ceram Soc. **36**, 655 (2016).
9. C. Y. Ma, F. Tang, J. F. Zhu, Z. C. Wen, Y. Yu, K. Wang, M. M. Du, J. T. Zhang, J. Q. Long, X. Y. Yuan, W. Guo, and Y. G. Cao, J. Eur. Ceram Soc. **36**, 2555 (2016).
10. C. Y. Ma, J. F. Zhu, Z. Q. Hu, Z. C. Wen, J. Q. Long, X. Y. Yuan, and Y. G. Cao, IEEE Photon. J. **9**, 1501814 (2017).
11. D. Y. Yan, P. Liu, X. D. Xu, J. Zhang, D. Y. Tang, and J. Xu, Opt. Mater Express **7**, 1374 (2017).
12. Z. Y. Zhou, Y. Wang, B. Xu, H. Y. Xu, Z. P. Cai, X. D. Xu, D. Z. Li, and J. Xu, Opt. Mater. **70**, 11 (2017).
13. S. Qiao, Y. Zhang, X. Shi, B. Jiang, L. Zhang, X. Cheng, L. Li, J. Wang, and L. Gui, Chin. Opt. Lett. **13**, 051602 (2015).
14. Y. Kuwano, K. Suda, N. Ishizawa, and T. Yamada, J. Cryst. Growth **260**, 159 (2004).
15. X. D. Xu, X. D. Wang, J. Q. Meng, Y. Cheng, D. Z. Li, S. S. Cheng, F. Wu, Z. W. Zhao, and J. Xu, Laser Phys. Lett. **6**, 678 (2009).
16. Q. Liu, M. L. Gong, T. H. Liu, Z. Sui, and X. Fu, Opt. Lett. **41**, 5322 (2016).
17. R. L. Aggarwal, D. J. Ripin, J. R. Ochoa, and T. Y. Fan, J. Appl. Phys. **98**, 103514 (2005).
18. J. Ma, T. T. Lu, P. X. Zhang, X. L. Zhu, Y. Hang, and W. B. Chen, Opt. Quantum Electron. **47**, 3213 (2015).
19. C. Pfistner, R. Weber, H. P. Weber, S. Merazzi, and R. Gruber, IEEE J. Quantum Electron. **30**, 1605 (1994).
20. L. M. Frantz and J. S. Nodvik, J. Appl. Phys. **34**, 2346 (1963).
21. L. Ding, Q. Zhang, J. Luo, W. Liu, W. Zhou, and S. Yin, J. Alloys. Compd. **509**, 10167 (2011).